Full Paper

Physicochemical investigation of nanostructured silica/wheat gluten hybrid materials prepared by catalytic sol-gel chemistry

Hasan Türe, Thomas O. J. Blomfeldt, Mikael Gällstedt, Mikael S. Hedenqvist, Stefano Farris*

_____

S. Farris, Dr.
Department of Food, Environmental and Nutritional Sciences (DeFENS), Packaging Division
University of Milan, Via Celoria 2, I–20133 Milan, Italy
E-mail: mikaelhe@kth.se
H. Türe, Dr. T. O. J. Blomfeldt, Dr. M. S. Hedenqvist, Prof.
Department of Fibre and Polymer Technology, KTH Royal Institute of Technology, SE–10044 Stockholm, Sweden
M. Gällstedt, Dr.
Innventia, Box 5604, SE–11486 Stockholm, Sweden

_____

In this work, the main physicochemical properties of nanostructured silica/wheat gluten hybrid composites are presented. The extraction experiments in different solvents suggest that the protein phase is intimately encased within the silica matrix, with silica-protein interactions driven by hydrogen bonding, as indicated by IR spectra. Spectroscopic results also show that the presence of silica induces a higher degree of constraint of the wheat gluten matrix, despite less aggregation. Moisture diffusion properties of the hybrid materials are investigated by a combined "desorption/sorption" approach. While the reduction of the moisture diffusivity in the presence of silica could be described by the geometrical impedance of a "sintered" porous solid, a time-dependent relaxation/restructuring of the composite apparently occurs during the complete sorption-desorption cycle, leading to a time-dependent increase in diffusivity.

Introduction

Over the last few decades, increased environmental concern has prompted a renewed interest in renewable resources. Economical, legislative, and market factors have been specifically identified as the main forces behind this trend.[1] In light of this, the ability to improve the overall properties of already available renewable and/or biodegradable polymers has become a priority research area. In particular, improving key properties such as barrier, mechanical, thermal, and dielectric properties without jeopardizing the inherent degradability/recyclability of the starting polymer remains a major challenge. Consequently, several types of biopolymers have been investigated.[2]

However, some drawbacks still hinder the full exploitation of most biopolymers. Among others, high sensitivity to moisture, poor barrier properties, and unsatisfactory mechanical performance have been indicated as limiting factors.[3] To date, many different approaches have been used to address these limitations, especially to improve the resistance to moisture, including thermal treatment-mediated polymer network modifications; the use of mixed wheat gluten and hydrophobic biodegradable polymers (e.g., polycaprolactone); or incorporation of nanofillers such as montmorillonite.[4] Growing interest in nanoscale organic-inorganic hybrid network polymer materials represents a more recent booster for the exploration of new bulk and thin-film reaction mechanisms.[5] In particular, the design of "bottom-up" architectures from a molecular precursor via the sol-gel processing has been proven to be a versatile and rather easy route to generate materials with previously non-achievable properties.[6]

Wheat gluten (WG) is one of the most promising materials of natural origin because of its wide availability and low cost. In fact, the availability of WG is expected to increase in the future, since it is a byproduct of starch production for ethanol biofuel, the consumption of which is forecast to increase over the next few years.[7] However, gluten-based materials are highly sensitive to moisture. This is primarily due to the inherent hydrophilic nature of the

WG protein as well as the substantial amount of hydrophilic plasticizer (e.g., glycerol) generally added to impart adequate film flexibility.[8]

In the present study, we propose the sol-gel chemistry as an alternative approach for the fabrication of silica/wheat gluten hybrid materials. To this scope, a metal alkoxide (i.e., tetraethyl orthosilicate, TEOS) was used as a precursor for in situ, acid-catalyzed development of silicon dioxide as the inorganic part of the final hybrid network. This approach has already been adopted to produce hybrid silica-based materials for the controlled release of entrapped active agents,[9] to obtain biodegradable composite scaffolds for bone tissue engineering,[10] to design hybrid membranes for uptake of metal ions,[11] or for the fabrication of hybrid nanoparticles with tailored interfacial properties and colloidal behavior,[12] just to provide a few examples. Very recently, our research group developed a high-oxygen barrier hybrid coating according to the aforementioned approach.[13] Moreover, the feasibility of combining alkoxysilanes with wheat gluten has previously been demonstrated.[14,15] Here, we discuss for the first time the changes induced by the presence of silica on the protein structure, and what role the final co-existing silica and wheat gluten structures have on material properties. Special focus is devoted to the moisture diffusion since it is a sensitive probe to changes in the actual geometry of the inorganic component in the hybrid material as well as to changes in the molecular mobility of the penetrable gluten component.

Experimental Section

Reagents and Chemicals

The commercial WG powder was kindly supplied by Lantmännen Reppe AB, Sweden. According to the supplier, the gluten protein content was 77.7 wt% (dry basis) (modified

NMKL Nr 6, Kjeltec, N×5.7, www.NMKL.org), the moisture content was 6.9 wt% of the total weight (NMKL 23, 1991), and the starch content was 5.8 wt% (dry basis) (Ewers, polarimetric method). The concentration of fats was 1.2 wt% (dry basis) (Soxtec, Lidfett.OA.19, tecator AN 301), and the residual ash content was 0.9 wt% (dry basis) (NMKL 173 2nd ed). The wheat gluten particle size distribution was: 10% between 160-250 µm; 20% between 100-160 µm; 55% between 50-100 µm; and 15% <50 µm. Tetraethoxylane (TEOS, reagent grade 98%), 1 M hydrochloric acid, anhydrous acetic acid (purity: 98.0%), sodium sulphite (purity: 98.0%), and ethanol (purity: 99.0%) were purchased from Sigma-Aldrich. Milli-Q water (18.3 MΩ·cm) was also used during the preparation of the WG and WG/silica materials. All reagents were used as received.

Preparation of Hybrid Films

In the first step, an acidic water solution (pH = 2.0 ± 0.2) was prepared using 1M HCl as the catalyst for the successive TEOS hydrolysis. In this step, the H_2O:TEOS molar ratio was fixed at 2:1. Then, ethanol was added to the same water solution (30 wt.% ethanol) to allow miscibility between TEOS and water.[16] The hydrolysis reaction of TEOS was carried out in a glass flask under magnetic stirring (~ 1000 rpm) at room temperature during about 30 min. An aqueous dispersion of wheat gluten was prepared at room temperature by mixing gluten powder with water containing sodium sulphite (2.5 mg/g wheat gluten), for 30 min. As an example, the preparation of a WG/SiO_2 1:1 is reported here: 21.68 g TEOS were added to a hydroalcholic solution containing 14.9 g ethanol and 3.75 g acidic water and left reacting according to the aforementioned conditions for the hydrolysis to occur. 10 g of WG powder were dissolved in 49.67 of distilled water using 25 mg sodium sulphite. The inorganic and organic phases were then mixed together for 1 h (100 rpm at room temperature) to facilitate the formation of the hybrid network. To investigate the influence of the organic/inorganic

ratio (O/I, defined as the wheat gluten/$(SiOH)_4$ weight ratio, assuming complete hydrolysis) on the final properties of the composites, five different hybrid materials were prepared by varying the O/I ratio from 3.0 to 0.5 (**Table 1**). Note that subscripts indicate the O/I ratio (for example, H_3 refers to the hybrid material with O/I=3). WG and hybrid materials were obtained by pouring a constant amount (16 g) of hydro-alcoholic dispersions onto plastic Petri dishes ($\varnothing$=6 cm), which were then stored in an oven at 40°C for 24 h. The films were stored in desiccators over silica gel for at least two weeks before analysis.

Characterization of the Hybrid Materials

Infrared Spectroscopy

A Perkin-Elmer Spectrum 2000 FTIR spectrometer (PerkinElmer, Waltham, USA) equipped with a single-reflection Golden Gate™ attenuated total reflectance (ATR) accessory (Specac Ltd., Kent, UK) was used. Spectra were recorded as an average of 16 scans between 4000 and 600 cm^{-1}, at intervals of 1 cm^{-1} and with a resolution of 4 cm^{-1}. Three replicates were used for each formulation.

Immersion Experiments

Both pure WG and hybrid film samples (5 g) were immersed in three different solvents: distilled water, ethanol (96 vol.%; VWR International S.A.S), and sodium dodecyl sulfate (SDS, 20 vol.%; Fluka, Buchs) contained in 20 mL glass vials. Experiments were carried out at room temperature and under static conditions (i.e. without stirring), and the degradation/solubility of the samples was monitored over a period of 107 days. Three replicates were considered for each sample.

Sorption and Desorption Experiments and Numerical Analysis

For sorption and desorption experiments, samples in the form of planar sheets were initially stored at 23°C in a desiccator over silica gel for two weeks. The thickness of each specimen used in the sorption modeling was then measured with a micrometer (Mitutoyo IDC-112B, Mitutoyo Scandinavia AB, Sweden) to the nearest 0.001 mm at 10 different random locations. The same samples were finally transferred to a climate room kept at 23 ± 0.5°C and 50 ± 2.0% RH, and the mass uptake was recorded as a function of time. Once the equilibrium mass uptake was attained, the samples were again stored in a desiccator over silica gel. The mass loss as a function of time was recorded by intermittently removing the samples from the desiccator and weighing them. The thickness used in the desorption modeling was measured on the swollen sample prior to the desorption experiment.

The desorption data was fitted using a concentration dependent diffusivity:

$$D(C) = D_{co}e^{\alpha C} \tag{1}$$

where D_{co} is the zero moisture concentration diffusivity and α is the plasticisation power. Fick's second law of diffusion, which can be expressed as

$$\frac{\partial C}{\partial t} = \frac{\partial}{\partial x}\left(D(C)\frac{\partial C}{\partial x}\right) \tag{2}$$

was solved for a plate geometry where C is the penetrant concentration (g cm^{-3}), x is the thickness coordinate, and t is time. Only half the plate thickness was considered, and the inner boundary coordinate was described as an isolated point. At the outer boundary, the concentration of moisture was considered to be zero. The numerical procedure for solving Equation 2 has been presented elsewhere and is only briefly described here.[17,18] By first implementing Equation 1 in Equation 2, Equation 2 can be discretized according to:

$$\frac{\partial C}{\partial t} = f(t, C) = \frac{D_{CO}}{\Delta x_i^2}\left(e^{\alpha C_{i+0.5}}(C_{i+1} - C_1) - e^{\alpha C_{i-0.5}}(C_i - C_{i-1})\right) \tag{3}$$

where

$$C_{i \pm 0.5} = \frac{C_i + C_{i \pm 1}}{2} \tag{4}$$

The concentration profiles were generated with an implicit multi-step method:[18]

$$\nabla^3 C_{j+1} = \frac{6}{11} h_j \left(f(t_{j+1}, C_{j+1}) - \frac{1}{h_j} \left(\frac{3}{2} \nabla^2 C_j + \nabla C_j \right) \right) \tag{5}$$

which was derived from the multi-step formula:[19]

$$\frac{1}{3} \nabla^3 C_{j+1} + \frac{1}{2} \nabla^2 C_{j+1} + \nabla C_{j+1} = h_j f(t_{j+1}, C_{j+1}) \tag{6}$$

where C_{j+1} is calculated from:

$$C_{j+1} = \nabla^3 C_{j+1} + \nabla^2 C_j + \nabla C_j + C_j \tag{7}$$

using the Nordsieck matrix of differences ($\nabla^3 C_{j+1} = \nabla^2 C_{j+1} - \nabla^2 C_j$ etc).[19] The implicit method integrates with respect to time using arcs with three constant time steps but with a variable step size between them. After the last step of each arc, the local error is estimated and a new step size is selected. The predictor-corrector procedure for solving the implicit Equation 5 was of the Newton-type. Matlab® (The Mathworks Inc., Natick, MA, USA) was the software used throughout the modeling procedure.

Thermal Properties

Thermogravimetric analysis (TGA) was carried out using a Mettler Toledo SDTA 851^e. Film samples (~ 5 mg) were placed in alumina pans (70 μL) and first kept at 25°C for 10 min, after which they were heated up to 800°C at a rate of 10°C min^{-1} in both an inert (50 mL min^{-1} N$_2$) and an oxidizing (50 mL min^{-1} O$_2$) environment. Three replicates were used for each sample.

Scanning Electron Microscopy Analysis

Field-emission scanning electron microscopy (FE-SEM) images were collected using a Hitachi S-4800 FE-SEM. Ashes collected immediately after the TGA run were mounted with

carbon tape on stubs. Before insertion in the microscope, the film samples were coated with gold to a thickness of ~ 10 nm using an agar high-resolution sputter coater (model 208RH) equipped with a gold target/agar thickness monitor controller.

Statistical Analysis

Data were analyzed using Statgraphics Plus 4.0 software (STSC, Rockville, MD, USA), and one-way analysis of variance was used to check for differences between samples. Mean values, when appropriate, were separated by LSD's multiple range test at $p < 0.05$.

Results and Discussion

WG-Silica Hybrid Formation as Revealed by IR

IR of pristine wheat gluten and reacted TEOS are reported in **Figure 1 (a)** and **Figure 1 (b)**, respectively, whereas the three main spectral regions of the hybrid materials are displayed in **Figure 1 (c)-(e)**. In the first region 3780–2500 cm^{-1} (**Figure 1 (c)**), a decrease in the O/I ratio resulted in a broadening of the band assigned to amide A and B (N-H stretching vibration) of WG, which has been ascribed to extensive hydrogen bonding between the silanol and hydroxyl/amine/amide groups of the organic phase.[20,21]

The second region (1840 cm^{-1}–1325 cm^{-1}, **Figure 1 (d)**) contains the two strong protein bands: amide I and amide II, the peak intensities of which are directly influenced by the backbone conformation (the secondary structure of the protein). More specifically, the bands at 1651 cm^{-1} and 1644 cm^{-1} can be assigned to the α-helices/random coils and disordered domains, respectively, while the bands at 1635 cm^{-1} and 1625 cm^{-1} are attributed to β-sheets with a high and low level of hydrogen bonding, respectively.[22] The addition of the inorganic phase reduced the intensity in the region from ~1640 cm^{-1} to ~1620 cm^{-1} relative to the

intensity of the peaks at 1644 cm^{-1} and 1651 cm^{-1} (see the inset in **Figure 1 (d)**). These observations demonstrated that the presence of the inorganic phase favored the presence of unordered and α-helix structures at the expense of β-sheets. Hence, it appeared as if the aggregation of the protein was lower in the presence of silica.

The third region (1340 cm^{-1}-700 cm^{-1}, **Figure 1(e)**) can be used as a diagnostic tool to assess possible interactions involving the inorganic phase. In this region, the band centered at ~945 cm^{-1}, assigned to silanol groups, shifts toward higher wavenumbers, with the largest shift observed for the H$_3$ formulation (peak centered at 962 cm^{-1}). The extent of this shift was gradually reduced as the O/I ratio was decreased until finally, for sample H$_{0.5}$, no shift was observed. The extensive hydrogen bonds formation was also confirmed by the shifting of the peak assigned to the silicon dioxide (SiO$_2$) asymmetric stretching (~1060 cm^{-1}) toward lower wavenumbers as the O/I ratio decreased (down to 1040 cm^{-1} for the sample H$_{0.5}$).

Immersion Experiments

The resistance of the hybrid materials to liquid environments was tested directly by soaking the samples in distilled water and using pure WG samples as a reference. For clarity, only the comparison between the pure WG material and the hybrid H$_1$ is shown in **Figure 2**, although the H$_3$ hybrid was also tested. After 24 h, the pure WG sample was already no longer able to stand due to plasticization of the matrix (**Figure 2**, left column). The effect of the water molecules (partly dissolving the matrix) was further enhanced after 60 days of analysis, when the original structure turned into a thick sediment at the bottom of the vial. In contrast, the hybrid film did not show any sign of failure throughout the experiment when it was in contact with water, although it swelled. It was thus decided to conduct the same experiment using sodium dodecyl sulfate (SDS), which is known to disrupt non-covalent (secondary) bonds within the gluten network, specifically hydrophobic interactions.[23] As shown in **Figure 2**

(middle column), the pure WG material was completely dissolved after two months, confirming that i) the use of SDS (20 wt.%) allowed not only the disruption of hydrogen bonds, as in the case of distilled water; and ii) the pure WG material was a physical network, i.e., inter-molecular disulfide bonds were not present to such an extent that the structure remained intact despite the SDS treatment.

In contrast, the hybrid material under the same conditions retained full integrity even after two months. Assuming that no covalent bond formation occurred between WG and silica (no clear evidence can be gathered from the IR analysis), these results can be explained by assuming a more constrained, less accessible organization of WG mediated by the inorganic phase, as will be discussed later. Finally, in contact with ethanol both pure WG and hybrid films swelled only slightly, but cracks developed (**Figure 2**, right column). It should be mentioned that the H_3 sample behaved like the H_1 sample in the different liquids. The swelling and subsequent loss of material was measured on the H_3 sample. After 107 days of exposure to water, SDS, and ethanol, the mass uptake was 52%, 82%, and 6%, respectively. After 30 days in a desiccator over silica gel, the mass loss relative to the initial mass, after the exposure to water, SDS, and ethanol, was 40%, 38%, and 4%, respectively. Since the initial content of WG in H_3 was 75%, it is evident that water and SDS were able to remove approximately half of the wheat gluten part. As mentioned before, this suggests that the solution had problems reaching into the interior of the hybrid material due to the inorganic phase.

TGA and SEM

The results arising from the thermal gravimetric analysis are summarized in **Figure 3**, in which only the three representative samples WG, H_1, and $H_{0.5}$ are shown. **Figure 3 (a)** depicts the traces obtained from the samples exposed to an inert environment. It can be seen that the degradation of the pure WG sample occurred in two main temperature regions, i.e. at 210°C–

255°C and 280°C—480°C, which accounted for approximately 80% of the total weight loss. In the hybrid composites H_1 and $H_{0.5}$, the first region disappeared and the total weight loss (~ 34% and ~ 50%, respectively) was limited to the second temperature range. The first-order derivatives of the TGA curves more clearly revealed that, with the exception of the first degradation peak at 215°C for the WG sample, the maximum decrease in mass occurred at ~320°C for all the three materials. This observation includes all the other formulations not shown in the figure. The different peak intensity reflects the decreasing amount of the organic phase in samples H_1 and $H_{0.5}$, which degraded less upon heating. To further study the thermal stability of the different materials, we decided to run the TGA analysis in O_2 (**Figure 3 (b)**). At first glance, a more complex pattern can be observed, owing to the greater complexity of the combustion process compared to the pyrolysis process. In particular, approximately 55% weight loss of the pure WG material took place between 220°C and 425°C. The presence of many subsequent peaks in the first-order derivative plot suggests that functionalities of the protein primary structure degraded under specific mechanisms, such as elimination-type reactions already observed for the hydroxyl groups of synthetic polymers.[24] The remaining ~43% loss due to two distinct degradation processes centered at ~510°C and ~636°C could be due to decomposition of the main protein chain. However, these hypotheses should be confirmed by additional data.

The addition of silica into the organic network led to a less pronounced degradation step between 250°C and 370°C, with a second combustion stage between 450°C and 630°C. More noticeably, the peak associated with the main second combustion step shifted toward higher temperatures (from ~510°C to ~565°C) for the hybrid samples. This "protective" role of silica was also confirmed by the SEM images collected from the samples immediately after the TGA experiments. Although fractures eventually developed, the hybrid materials kept their original size/structure. The fracture surface of a sample after the N_2-TGA run revealed a diffuse network with dots (**Figure 4 (a)**). The structures of the hybrid materials after the O_2-

TGA runs are shown in **Figure 4 (b)** to **4 (d)**, which show that the silica forms a continuous network in the hybrid. Hence, the in-situ formation of silica in the presence of WG yields an interpenetrating network in which the uncondensed silanol group of the glass-like oxidic network interacted via hydrogen bonding with groups of the most abundant wheat gluten amino acids (e.g., –OH and –NH$_2$ groups of glutamic acid, aspartic acid, serine, threonine, asparagine, arginine, and lysine).[25] Based on these results, the addition of silica to the organic phase appeared to be a promising approach for the development of hybrid materials with improved heat-resistance properties, although our data clearly reflected effects concerning only rather high temperatures.

Mass Transport Properties

Figure 5 (a) shows the sorption curves for WG and H$_3$. Notably, the WG curves went through a maximum followed by a decrease before a steady-state was attained. Presumably, when the samples were hydrated at 50% RH, the sample was aggregating further and thereby "sweating" out/releasing moisture, due to the well-known moisture-induced protein aggregation. This phenomenon has been already observed and widely discussed for other protein systems, such as insulin,[26,27] whey proteins,[28] and α-lactalbumin,[29] and has been linked to small structural changes as a consequence of moisture sorption. In particular, moisture sorption leads to greater conformational flexibility of the protein molecules, which enables structural transitions especially on the tertiary structure, eventually leading to protein aggregation, mainly driven by noncovalent interactions (although covalent interactions such as intermolecular disulphide bonds has been also postulated). Note that this phenomenon was absent in the presence of silica. The hypothesis is that the addition of the inorganic phase prevented significant reaggregation of the protein due to silica-WG interactions. A similar phenomenon was described for α-lactalbumin,[29] where the addition of calcium ions

significantly improved the thermal stability of the protein and slowed down the formation of protein aggregates. Similarly, the addition of silica induced strong interactions mediated by hydrogen bonding, which would have eventually restricted the segmental mobility of the molecular chains within the amorphous regions, thus reducing the degree of unfolding of the protein, even during moisture uptake.

All the sorption curves were s-shaped in the uptake region, indicative of the build-up and release of swelling-induced internal stresses, a common feature in highly swelling systems.[18] This fact, and the decrease in moisture content with increasing time observed for WG, made it difficult to interpret the sorption kinetics. Therefore, before analysing the sorption data further, the desorption data was analyzed first. **Figure 5 (b)** gives examples of fits of the desorption data using Equation 1. The following data were obtained: WG: $D_{co}=15.5\pm5\cdot10^{-10}$ cm^2 s^{-1} and $\alpha=63\pm4$ g polymer/g solute, H$_3$: $D_{co}=7\pm1\cdot10^{-10}$ cm^2 s^{-1} and $\alpha=58\pm5$ g polymer/g solute. The zero-concentration diffusivity reflects the differences in both the geometrical impedance of the structure and the mobility of the penetrable portion of the composite. Since the plasticisation power, which is generally larger for a more constrained system, was insignificantly different for the two systems, D_{co} probably reflected mainly the geometrical impedance imposed by the presence of the impermeable silica component. The measured ratio (R) in D_{co} between WG and H$_3$ was 2.2. This can be compared with a theoretical value considering a co-continuous silica-WG material using the relationship by Weissberg:[30]

$$R = 1 - 0.5\ln(v) \tag{8}$$

where v is the volume fraction of silica, which is 0.14 for H$_3$, considering a weight fraction of 0.25 and using 1.3 g cm^{-3} as the WG density[31] and 2.6 g cm^{-3} as the silica density.[32] In using the Weissberg equation, we equate our system with a system having a sintered impermeable solid phase surrounded by pores. The theoretical value of the ratio in D_{co} between WG and H$_3$ became 2.0, i.e., very close to the measured ratio.

The swelling-induced s-shaped sorption curves may be described with the same algorithms as used above [Equation (1)-(7)], but using a time-dependent outer surface concentration.[18] The boundary can be described as:

$$C(t) = C_{i2} + (C_\infty - C_{i2})\left(1 - e^{-\frac{t}{\tau}}\right)$$

(9)

where C_{ib} and C_∞ are, respectively, the initial and steady-state surface concentrations. The rate at which the surface concentration approaches C_∞ is determined by the relaxation time τ. The many adjustable parameters using Equation 9 together with Equation 1 make it difficult to find an optimal fit/solution. The strategy was therefore to use the parameters in Equation 1 determined from desorption data and to try to fit the sorption curves by adjusting the parameters in Equation 8. It was observed that changing only the parameters in Equation 8 did not yield a good fit to the data. An approximate estimation of the "average" sorption diffusivity was therefore estimated using the following formula:

$$D = \frac{0.0419}{\dfrac{t_{0.5}}{l^2}}$$

(10)

where $t_{0.5}$ is the time to reach half of the maximum concentration and l is the sample thickness. The values obtained were WG: $D = 3.8 \pm 0.3 \cdot 10^{-9}$ cm^2 s^{-1} and H$_3$: $D = 1.7 \pm 0.2 \cdot 10^{-9}$ cm^2 s^{-1}.

Interestingly, the ratio in D between WG and H$_3$ was identical to the one measured above from desorption data (2.2). Finally, to compare sorption and desorption data, Equation 10 was also used on the desorption data. The values were WG: $D = 6.5 \pm 1.9 \cdot 10^{-9}$ cm^2 s^{-1} and H$_3$: $D = 3.0 \pm 0.4 \cdot 10^{-9}$ cm^2 s^{-1}, giving a ratio in D of 2.1. The fact that D was consistently larger for the desorption data compared to the sorption data suggests that a time-dependent relaxation/restructuring of the composite occurred during the complete sorption-desorption cycle, leading to a time-dependent increase in diffusivity.
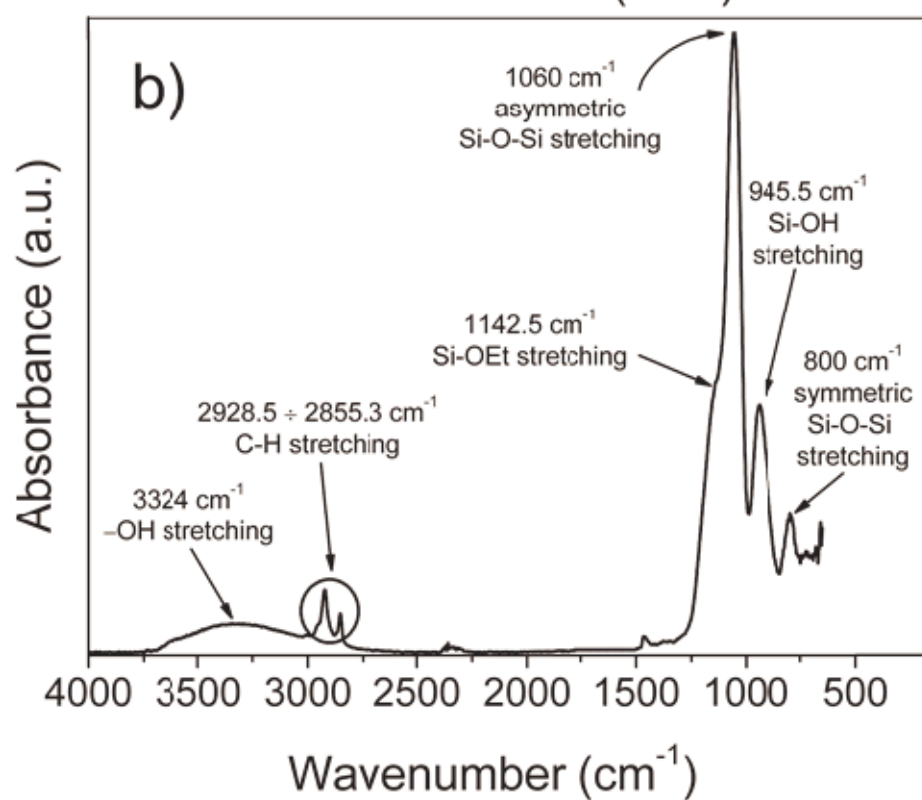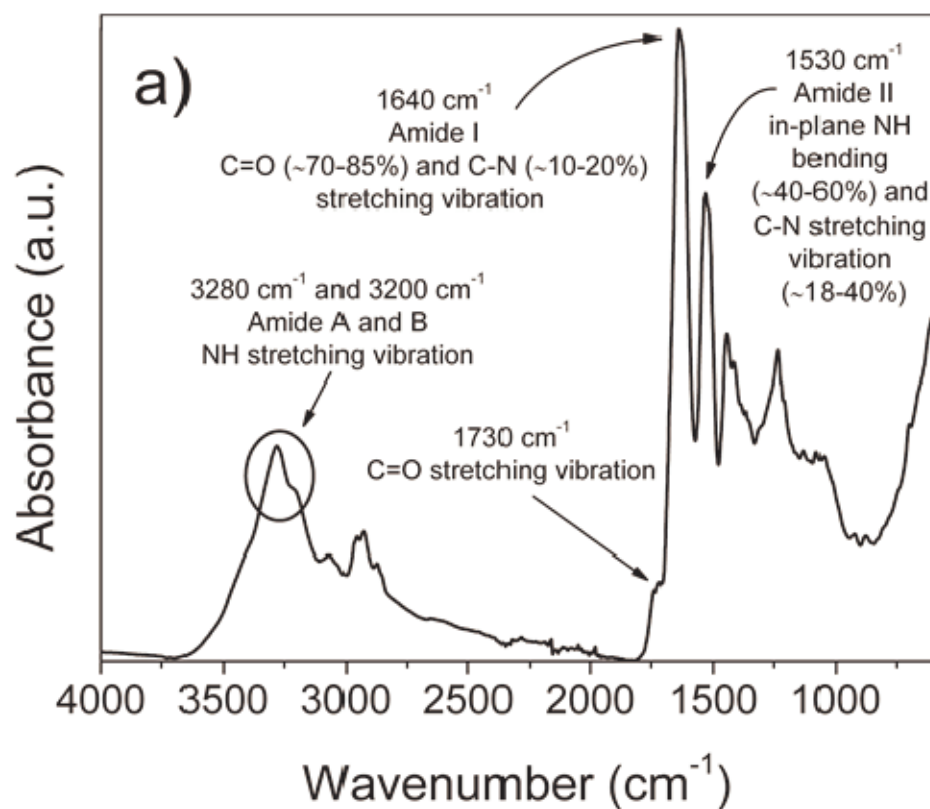
Conclusion

The presence of silica constrained the WG component to such an extent that moisture-induced aggregation/denaturation was small. A substantial improvement of the thermal properties as the silica content increased was also observed (e.g., the temperature of the second combustion step rose with 55°C in the presence of silica). Infrared spectroscopy and immersion data suggested that the constraint came from strong interactions between the silica and wheat gluten phases, mainly from hydrogen bond interactions. The constraint was, however, small enough not to affect the moisture diffusion; the plasticisation power α was similar in the WG and the H_3 materials. The reduction in moisture diffusivity in the presence of silica was fully explained by the geometrical impedance imposed by the interpenetrating silica phase. Hence, as was also shown by scanning electron microscopy, the acid-catalyzed in-situ polymerization of silica in the presence of wheat gluten generated an interpenetrating network with interesting, e.g., high-temperature, properties. An integrated approach that bridges different branches of chemistry (physical, organic, polymers, bio, and numerical), as shown in this work, can be the key towards new, functional, and "green" materials.
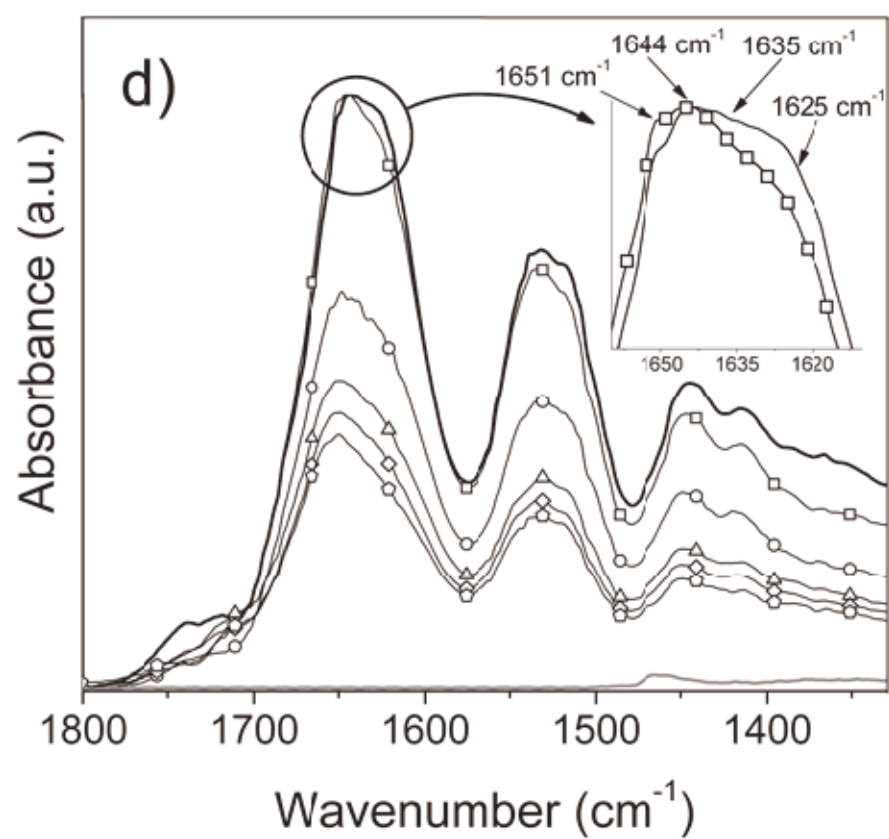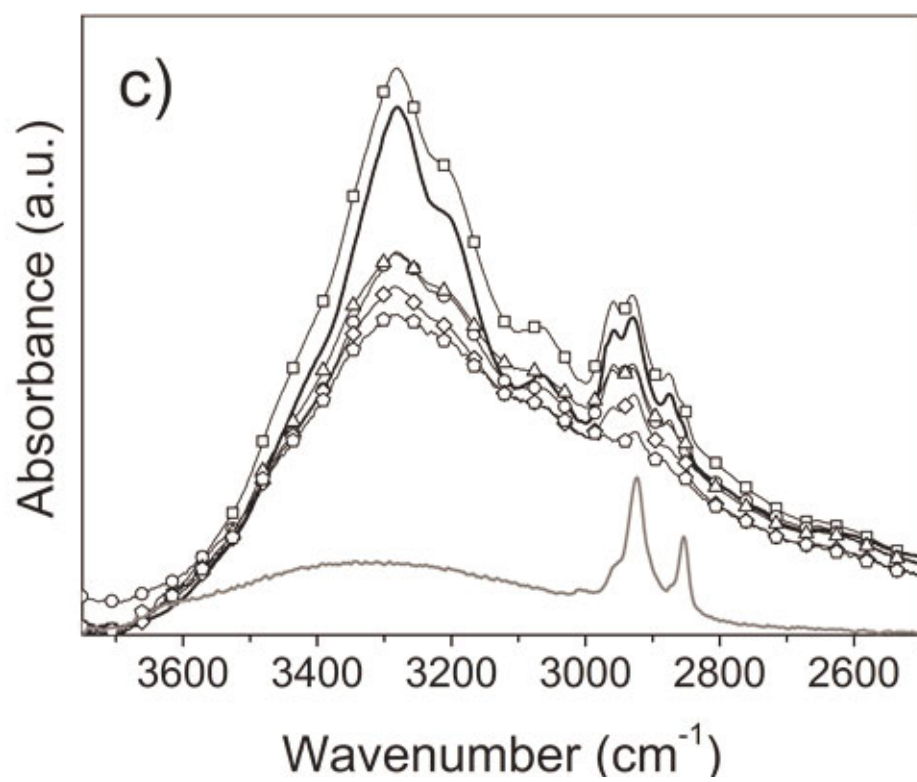
[1]   R. Coles, "Introduction", in *Food Packaging Technology*, R. Coles, D. McDowell, M. J. Kirwan, Eds., Blackwell Publishing Ltd., Oxford **2003**, pp. 1–31.

[2]   M. Gällstedt, A. Brottman, M. S. Hedenqvist, *Packag. Technol. Sci.* **2005**, *18*, 161.

[3]   L. Introzzi, T. O. J. Blomfeldt, S. Trabattoni, S. Tavazzi, N. Santo, A. Schiraldi, L. Piergiovanni, S. Farris, *Langmuir* **2012**, 28, 11206.

[4]   E. Mascheroni, V. Guillard, E. Gastaldi, N. Gontard, P. Chalier, *Food Control* **2011**, *22*, 1582.

[5]   B. Gong, Q. Peng, G.N. Parsons, *J. Phys. Chem. B* **2011**, *115*, 5930.

[6]   L. Nicole, L. Rozes, C. Sanchez, *Adv. Mater.* **2010**, *22*, 3208.

[7]   A. E. Farrell, R. J. Plevin, B. T. Turner, A. D. Jones, M. O'Hare, D. M. Kammen, *Science* **2006**, *311*, 506.

[8]   N. H. Ullsten, M. Gällstedt, E. Johansson, A. Gräslund, M. S. Hedenqvist, *Biomacromolecules* **2006**, *7*, 771.

[9]   H. O'Neill, S. M. Chathoth, M. B. Cardoso, G. A. Baker, E. Mamontov, V. S. Urban, *J. Phys. Chem. C* **2012**, *116*, 13972.

[10]   M. Peter, N. S. Binulal, S. V. Nair, N. Selvamurugan, H. Tamura, R. Jayakumar, *Chem. Eng. J.* **2010**, *158*, 353.

[11]   M. Irani, A. R. Keshtkar, M. A. Moosavian, *Chem. Eng. J.* **2012**, *200-202*, 192.

[12] K. Natte, W. Österle, J. F. Friedrich, R. von Klitzing, G. Orts-Gil, *Macromol. Chem. Phys.* **2012**, *213*, 2412.

[13]   S. Farris, L. Introzzi, J. M. Fuentes-Alventosa, N. Santo, R. Rocca, L. Piergiovanni, *J. Agric. Food Chem.* **2012**, *60*, 782.

[14]   X. Zhang, M. D. Do, A. Bilyk, *Biomacromolecules* **2007**, *8*, 1881.

[15]   S. Hemsri, A. D. Asandei, K. Grieco, R. S. Parnas, *Compos. Part A–Appl.* **2011**, *S. 42*, 1764.

 [16] M. Iotti, P. Fabbri, M. Messori, F. Pilati, P. Fava, *J. Polym. Environ.* **2009**, *17*, 10.

[17] M. S. Hedenqvist, M. Krook, U. W. Gedde, *Polymer* **2002**, *43*, 3061.

[18] M.S. Hedenqvist, U.W. Gedde, *Polymer* **1999**, *40*, 2381.

[19] E. Hairer, S. P. Nørsett, G. Wanner, *Solving ordinary differential equations*, Springer, Berlin **1993**.

[20] A. Bandyopadhyay, M. De Sarkar, A. Bhowmick, *J. Mater. Sci.* **2005**, *40*, 5233.

[21] S. Krimm, J. Bandekar, Adv. *Protein Chem.* **1986**, *38*, 181.

[22] S. W. Cho, M. Gällstedt, E. Johansson, M. S. Hedenqvist, *Int. J. Biol. Macromol.* **2011**, *48*, 146.

[23] I. Olabarrieta, S. W. Cho, M. Gällstedt, J. R. Sarasu, E. Johansson, M. S. Hedenqvist, *Biomacromolecules* **2006**, *7*, 1657.

[24] J. W. Gilman, D. L. Van der Hart, T. Kashiwagi, *Fire and polymers II: materials and test for hazard prevention*, American Chemical Society, ACS Symposium Series 599, Washington, D.C. **1994**.

[25] J. H. Woychik, J. A. Boundy, R. J. Dimler, *J. Agric. Food. Chem.* **1961**, *9*, 307.

[26] H. R. Costantino, R. Langer, A. M. Klibanov, *Pharm. Res.* **1994**, *11*, 21.

[27] G. M. Flores-Fernández, R. J. Solá, K. Griebenow, *J. Pharm. Pharmacol.* **2009**, *61*, 1555.

[28] P. Zhou, X. M. Liu, T. P. Labuza, *J. Agr. Food Chem.* **2008**, *56*, 2048.

[29] D. Liu, P. Zhou, X. Liu, T. Labuza, *J. Food Sci.* **2011**, *76*, 817.

[30] H. L. Weissberg, *J. Appl. Phys.* **1963**, *34*, 2636.

[31] S. W. Cho, M. Gällstedt, M. S. Hedenqvist, *J. Appl. Polym. Sci.* **2010**, *117*, 3506.

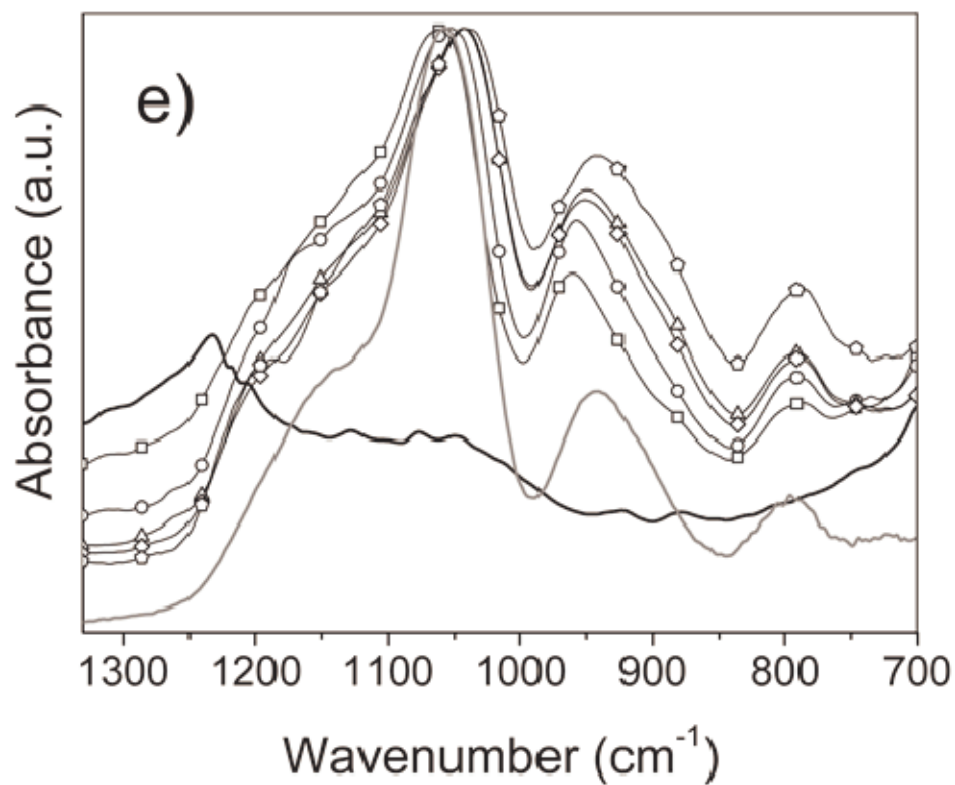[32] A. Wootton, B. Thomas, P. Harrowell, *J. Chem. Phys.* **2001**, *115*, 3336.

a)

1640 cm⁻¹
Amide I
C=O (~70-85%) and C-N (~10-20%) stretching vibration

1530 cm⁻¹
Amide II
in-plane NH
bending
(~40-60%) and
C-N stretching
vibration
(~18-40%)

3280 cm⁻¹ and 3200 cm⁻¹
Amide A and B
NH stretching vibration

1730 cm⁻¹
C=O stretching vibration

b)

1060 cm⁻¹
asymmetric
Si-O-Si stretching

945.5 cm⁻¹
Si-OH
stretching

1142.5 cm⁻¹
Si-OEt stretching

800 cm⁻¹
symmetric
Si-O-Si
stretching

2928.5 ÷ 2855.3 cm⁻¹
C-H stretching

3324 cm⁻¹
–OH stretching

c)

d)

1651 cm⁻¹ 1644 cm⁻¹ 1635 cm⁻¹ 1625 cm⁻¹

Figure 1. Normalized IR spectra of wheat gluten (a), reacted TEOS (b) and hybrid materials within 3780 cm^{-1} ÷ 2500 cm^{-1} (c), 1840 ÷ 1325 cm^{-1} (d), and 1340 cm^{-1} ÷ 700 cm^{-1} (e) spectral ranges. Symbols: (——) pure WG; (——) reacted TEOS; (–□–) H$_3$; (–○) H$_2$; (–△–) H$_1$; (–◇–) H$_{0.75}$; (—◁—) H$_{0.5}$. Each curve is the average of three replicates.
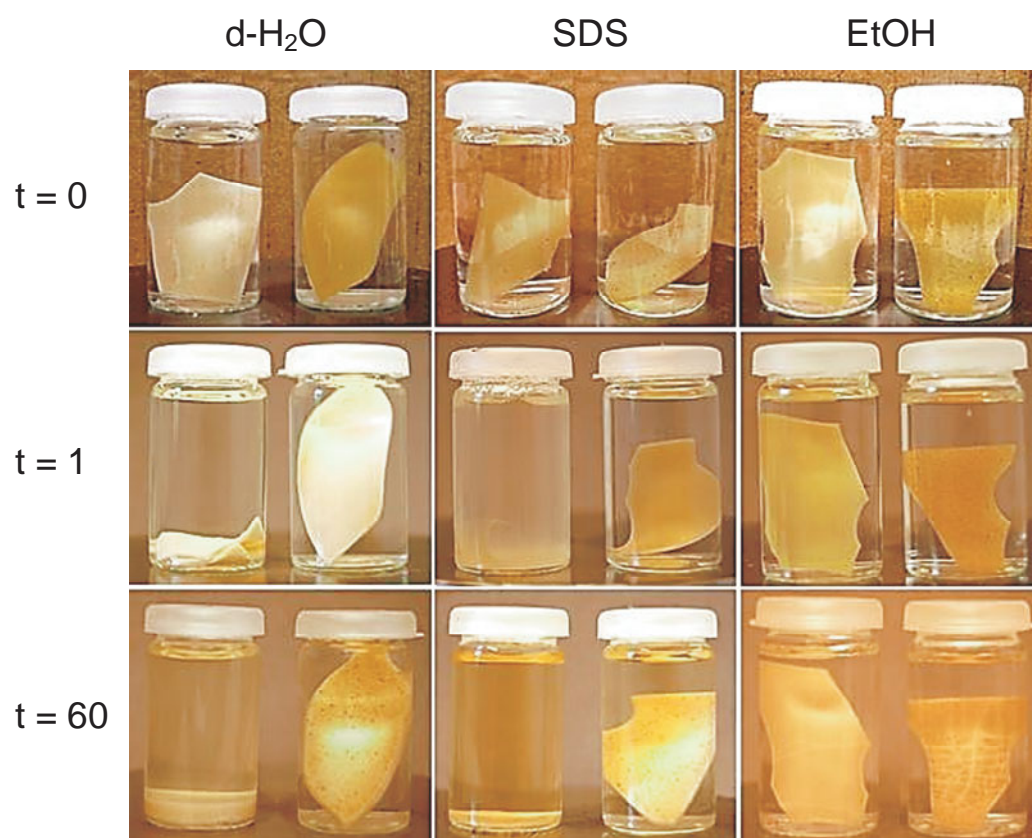
Figure 2. Pure WG (left vial) and wheat gluten-silica hybrid H_1 (right vial) materials in distilled water, sodium dodecyl sulfate, and ethanol immediately after immersion (t = 0) and after 1 day (t = 1) and 60 days (t = 60).
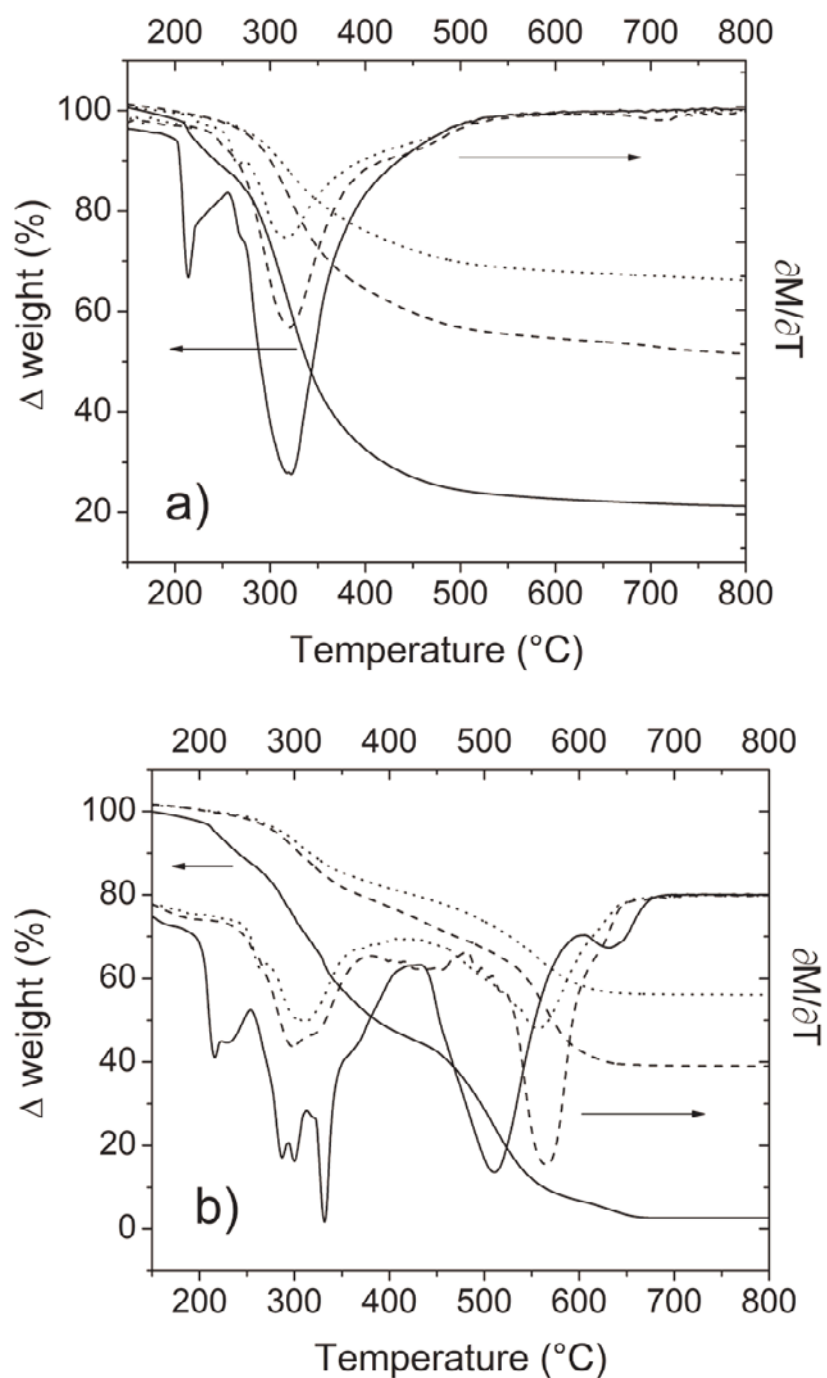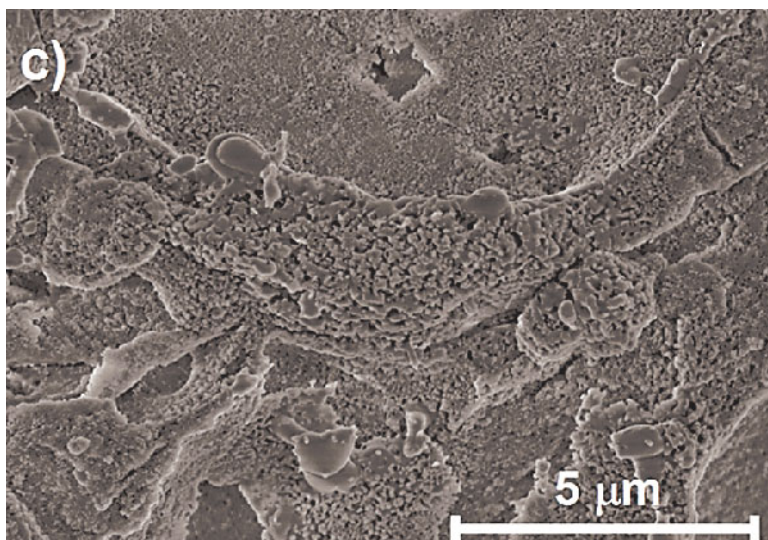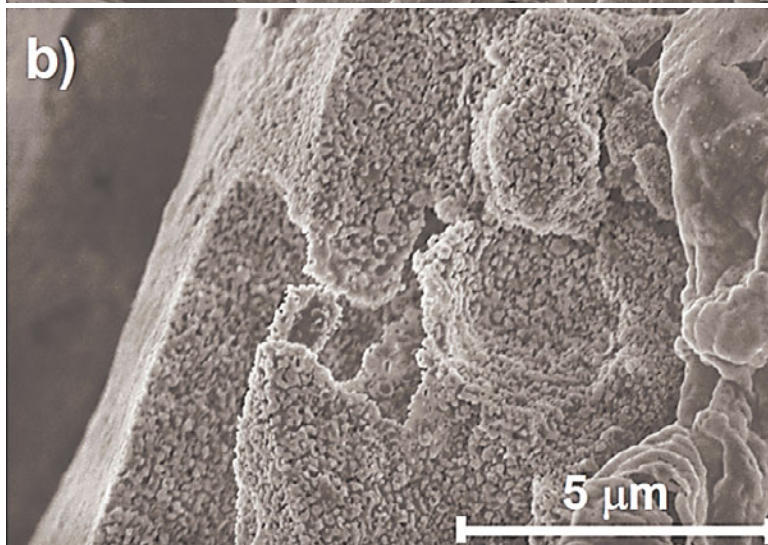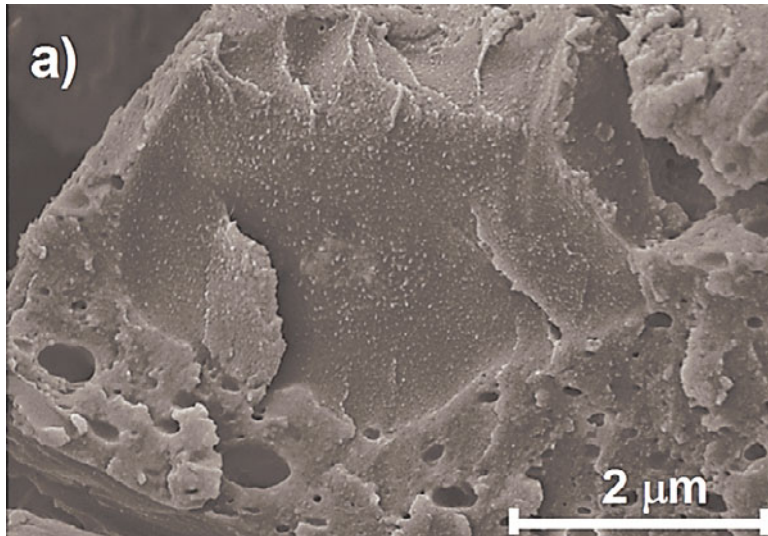
Figure 3. TGA traces and first-order derivatives of the same curves for the three representative materials WG (——), H_1 (- - - -), and $H_{0.5}$ (······) exposed to an N_2 (a) and an O_2 atmosphere (b).
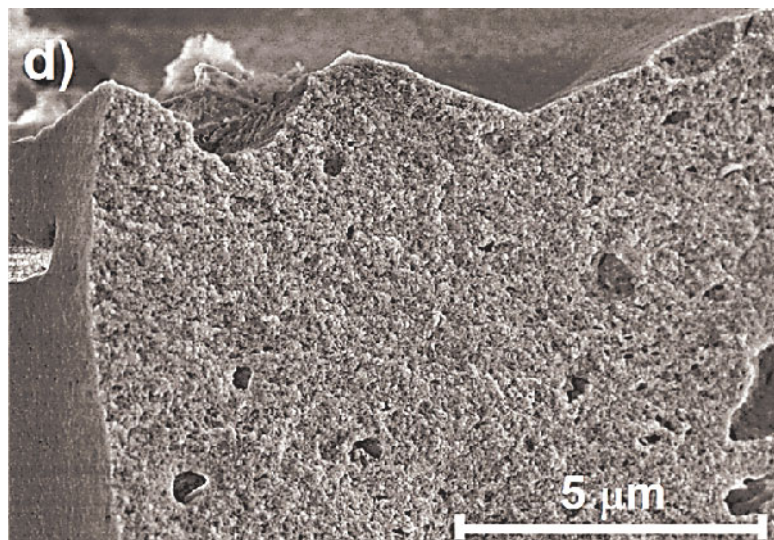
a)

b)

c)

Figure 4. SEM detail of a cross-sectional area of the hybrid H_1 after exposure to the high-temperature treatment during the TGA experiment under N_2 (a). SEM cross-sectional images of H_1 (b), H_2 (c), and H_3 (d) materials after exposure to the high-temperature treatment during the TGA experiment under O_2.
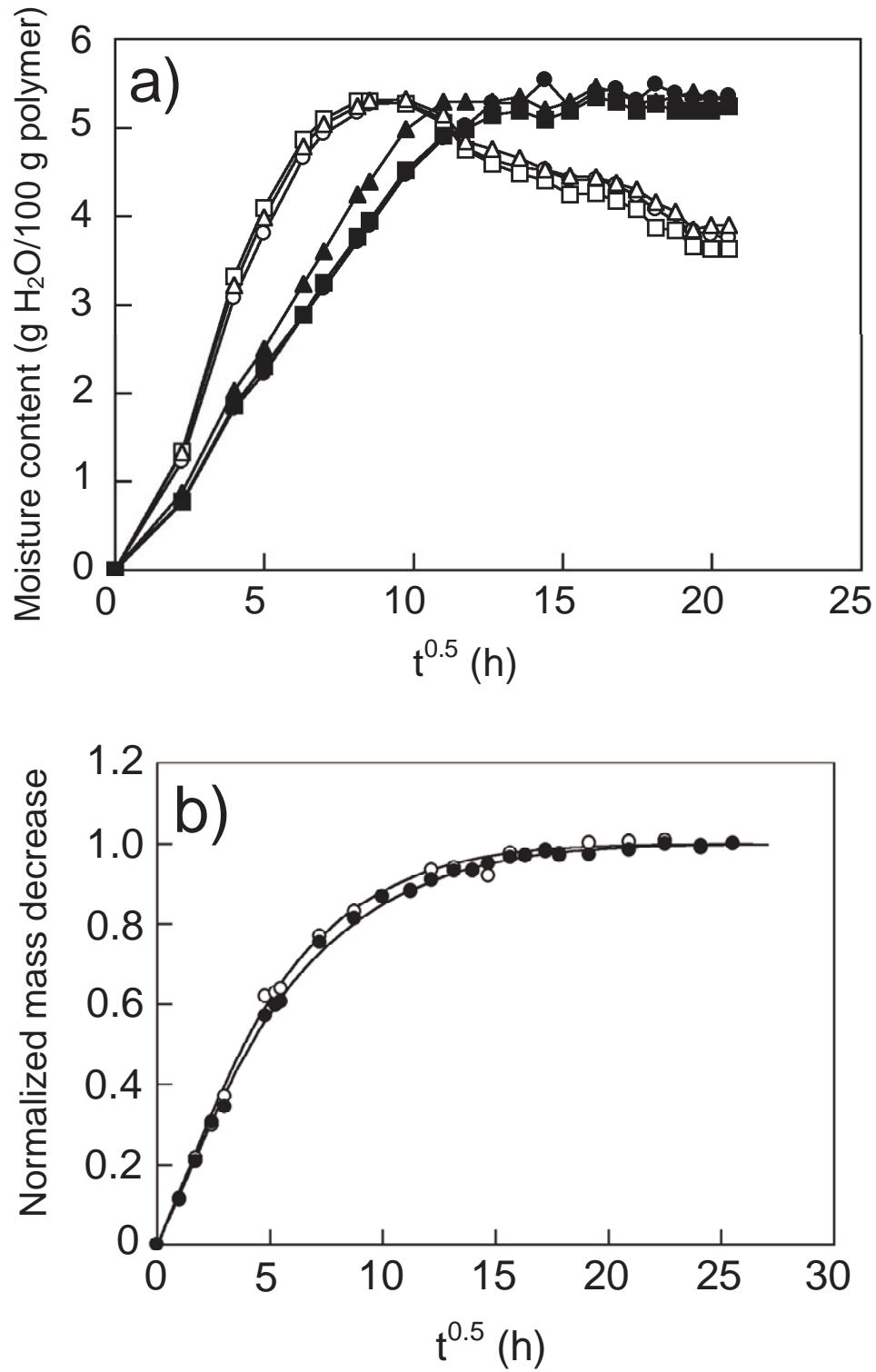
Figure 5. a) Experimental moisture sorption data for the WG material (open circles) and the H$_3$ hybrid composite (filled circles). The different symbols indicate individual data sets. b) Moisture desorption from a WG (open circles) and a H$_3$ (filled circles) sample. The solid line refers to the fitting of the model as described by Equation (1)-(7).

Table 1. Formulation of the pure WG and hybrid materials.

Coded name	WG [wt-%]	Si(OH)$_4$ [wt-%]	O/I ratio[a]
WG	20	0	/
H$_3$	15	5	3
H$_2$	13.32	6.66	2
H$_1$	10	10	1
H$_{0.75}$	8.6	11.4	0.75
H$_{0.5}$	6.66	13.32	0.5

[a] "I" refers to the silanol form – Si(OH)$_4$ calculated from the initial TEOS content and assuming the completion of the hydrolysis reaction.

An integrated physicochemical approach is used to produce silica/wheat gluten hybrid composites through sol-gel chemistry. Silica constrained the organic network, leading to enhanced thermal properties, whereas the constrain does not affect the moisture diffusion properties of the hybrid network. The reduced moisture diffusivity of the hybrid materials is explained in terms of geometric impedance.

H. Türe, T. O. J. Blomfeldt, M. Gällstedt, M. S. Hedenqvist, S. Farris*

Silica/wheat gluten hybrid materials

ToC figure